Downloaded from orbit.dtu.dk on: May 05, 2023

DTU Library

Coexistence of dissipative soliton and stretched pulse in dual-wavelength mode-locked Tm-doped fiber laser with strong third-order dispersion

Wang, Yazhou; Li, Jianfeng; Hong, Lujun; Li, Gaoyuan; Liu, Fei; Zhou, Xiaojun; Liu, Yong

Published in:
Optics Express

Link to article, DOI:
10.1364/OE.26.018190

Publication date:
2018

Document Version
Publisher's PDF, also known as Version of record

Link back to DTU Orbit

Citation (APA):
Wang, Y., Li, J., Hong, L., Li, G., Liu, F., Zhou, X., & Liu, Y. (2018). Coexistence of dissipative soliton and stretched pulse in dual-wavelength mode-locked Tm-doped fiber laser with strong third-order dispersion. *Optics Express*, *26*(14), 18190-18201. https://doi.org/10.1364/OE.26.018190

General rights
Copyright and moral rights for the publications made accessible in the public portal are retained by the authors and/or other copyright owners and it is a condition of accessing publications that users recognise and abide by the legal requirements associated with these rights.

- Users may download and print one copy of any publication from the public portal for the purpose of private study or research.
- You may not further distribute the material or use it for any profit-making activity or commercial gain
- You may freely distribute the URL identifying the publication in the public portal

If you believe that this document breaches copyright please contact us providing details, and we will remove access to the work immediately and investigate your claim.

Research Article | Vol. 26, No. 14 | 9 Jul 2018 | OPTICS EXPRESS 18190
Optics EXPRESS

Coexistence of dissipative soliton and stretched pulse in dual-wavelength mode-locked Tm-doped fiber laser with strong third-order dispersion

YAZHOU WANG,[1,2] JIANFENG LI,[1,*] LUJUN HONG,[2,3] GAOYUAN LI,[2] FEI LIU,[1] XIAOJUN ZHOU,[1] AND YONG LIU[1]

[1]*State Key Laboratory of Electronic Thin Films and Integrated Devices, School of Optoelectronic Information, University of Electronic Science and Technology of China (UESTC), Chengdu 610054, China*
[2]*DTU Fotonik, Technical University of Denmark, DK-2800 Kgs. Lyngby, Denmark*
[3]*Institute of Space Science and Technology, Nanchang University, Nanchang 330031, China*
[*]*lijianfeng@uestc.edu.cn*

Abstract: Mode-locked lasers with strong high order dispersion exhibit rich nonlinear dynamics. Here we numerically and experimentally demonstrate coexistence of dissipative soliton (DS) and stretched pulse (SP) in a dual-wavelength mode-locked Tm-doped fiber laser with strong third-order dispersion (TOD), where the DS and SP show completely different pulse duration and peak power. Wavelength-dependent feature of the net cavity group-velocity dispersion (GVD) leaded by the strong TOD plays a key role for the coexistence patterns. To our best knowledge, this is the first demonstration of the coexistence of different mode-locked pulse regimes with strong laser cavity TOD.

© 2018 Optical Society of America under the terms of the OSA Open Access Publishing Agreement

OCIS codes: (140.3510) Lasers, fiber; (140.3480) Lasers, diode-pumped.

References and links

1. L. E. Nelson, D. J. Jones, K. Tamura, H. A. Haus, and E. P. Ippen, "Ultrashort-pulse fiber ring lasers," Appl. Phys. B **65**(2), 277–294 (1997).
2. A. Cabasse, B. Ortaç, G. Martel, A. Hideur, and J. Limpert, "Dissipative solitons in a passively mode-locked Er-doped fiber with strong normal dispersion," Opt. Express **16**(23), 19322–19329 (2008).
3. N. Akhmediev and A. Ankiewicz, "Dissipative Solitons in the Complex Ginzburg-Landau and Swift-Hohenberg Equations," in *Dissipative Solitons*, N. Akhmediev and A. Ankiewicz, ed., (Springer, Berlin, 2005).
4. F. Ö. Ilday, J. R. Buckley, W. G. Clark, and F. W. Wise, "Self-Similar Evolution of Parabolic Pulses in a Laser," Phys. Rev. Lett. **92**(21), 213902 (2004).
5. K. Tamura, E. P. Ippen, H. A. Haus, and L. E. Nelson, "77-fs pulse generation from a stretched-pulse mode-locked all-fiber ring laser," Opt. Lett. **18**(13), 1080–1082 (1993).
6. D. Y. Tang, L. M. Zhao, G. Q. Xie, and L. J. Qian, "Coexistence and competition between different soliton-shaping mechanisms in a laser," Phys. Rev. A **75**(6), 063810 (2007).
7. P. Grelu and N. Akhmediev, "Dissipative solitons for mode-locked lasers," Nat. Photonics **6**(2), 84–92 (2012).
8. J. Herrmann, V. P. Kalosha, and M. Müller, "Higher-order phase dispersion in femtosecond Kerr-lens mode-locked solid-state lasers: sideband generation and pulse splitting," Opt. Lett. **22**(4), 236–238 (1997).
9. V. E. Zakharov and E. A. Kuznetsov, "Optical solitons and quasisolitons," J. Exp. Theor. Phys. **86**(5), 1035–1046 (1998).
10. J. M. Dudley, S. M. Boussen, D. M. J. Cameron, and J. D. Harvey, "Complete characterization of a self-mode-locked Ti:sapphire laser in the vicinity of zero group-delay dispersion by frequency-resolved optical gating," Appl. Opt. **38**(15), 3308–3315 (1999).
11. Y. Logvin, V. P. Kalosha, and H. Anis, "Third-order dispersion impact on mode-locking regimes of Yb-doped fiber laser with photonic bandgap fiber for dispersion compensation," Opt. Express **15**(3), 985–991 (2007).
12. Y. Logvin and H. Anis, "Similariton pulse instability in mode-locked Yb-doped fiber laser in the vicinity of zero cavity dispersion," Opt. Express **15**(21), 13607–13612 (2007).
13. H. A. Haus, J. D. Moores, and L. E. Nelson, "Effect of third-order dispersion on passive mode locking," Opt. Lett. **18**(1), 51–53 (1993).
14. V. L. Kalashnikov, A. Fernández, and A. Apolonski, "High-order dispersion in chirped-pulse oscillators," Opt. Express **16**(6), 4206–4216 (2008).

#330567 https://doi.org/10.1364/OE.26.018190
Journal © 2018 Received 3 May 2018; revised 3 Jun 2018; accepted 3 Jun 2018; published 29 Jun 2018

Optics EXPRESS

15. E. Sorokin, N. Tolstik, V. L. Kalashnikov, and I. T. Sorokina, "Chaotic chirped-pulse oscillators," Opt. Express **21**(24), 29567–29577 (2013).
16. L. Wang, "Coexistence and evolution of bright pulses and dark solitons in a fiber laser," Opt. Commun. **297**(15), 129–132 (2013).
17. X. Liu, "Coexistence of strong and weak pulses in a fiber laser with largely anomalous dispersion," Opt. Express **19**(7), 5874–5887 (2011).
18. S. Huang, Y. Wang, P. Yan, J. Zhao, H. Li, and R. Lin, "Tunable and switchable multi-wavelength dissipative soliton generation in a graphene oxide mode-locked Yb-doped fiber laser," Opt. Express **22**(10), 11417–11426 (2014).
19. L. Yun, X. Liu, and D. Mao, "Observation of dual-wavelength dissipative solitons in a figure-eight erbium-doped fiber laser," Opt. Express **20**(19), 20992–20997 (2012).
20. Z. X. Zhang, Z. W. Xu, and L. Zhang, "Tunable and switchable dual-wavelength dissipative soliton generation in an all-normal-dispersion Yb-doped fiber laser with birefringence fiber filter," Opt. Express **20**(24), 26736–26742 (2012).
21. H. Zhang, D. Y. Tang, X. Wu, and L. M. Zhao, "Multi-wavelength dissipative soliton operation of an erbium-doped fiber laser," Opt. Express **17**(15), 12692–12697 (2009).
22. Z. Yan, X. Li, Y. Tang, P. P. Shum, X. Yu, Y. Zhang, and Q. J. Wang, "Tunable and switchable dual-wavelength Tm-doped mode-locked fiber laser by nonlinear polarization evolution," Opt. Express **23**(4), 4369–4376 (2015).
23. M. Guina, N. Xiang, A. Vainionpää, O. G. Okhotnikov, T. Sajavaara, and J. Keinonen, "Self-starting stretched-pulse fiber laser mode locked and stabilized with slow and fast semiconductor saturable absorbers," Opt. Lett. **26**(22), 1809–1811 (2001).
24. H. T. Shang, "Chromatic dispersion measurement by white-light interferometry on metre-length single-mode optical fibres," Electron. Lett. **17**(17), 603–605 (1981).
25. H. Zhang, D. Y. Tang, L. M. Zhao, and N. Xiang, "Coherent energy exchange between components of a vector soliton in fiber lasers," Opt. Express **16**(17), 12618–12623 (2008).
26. F. Wang, A. G. Rozhin, V. Scardaci, Z. Sun, F. Hennrich, I. H. White, W. I. Milne, and A. C. Ferrari, "Wideband-tuneable, nanotube mode-locked, fibre laser," Nat. Nanotechnol. **3**(12), 738–742 (2008).
27. L. Xueming and L. Byoungho, "A fast method for nonlinear Schrodinger equation," IEEE Photonics Technol. Lett. **15**(11), 1549–1551 (2003).
28. G. Martel, C. Chédot, V. Réglier, A. Hideur, B. Ortaç, and P. Grelu, "On the possibility of observing bound soliton pairs in a wave-breaking-free mode-locked fiber laser," Opt. Lett. **32**(4), 343–345 (2007).
29. S. Kelly, "Characteristic sideband instability of periodically amplified average soliton," Electron. Lett. **28**(8), 806–807 (1992).
30. B. G. Bale, S. Boscolo, and S. K. Turitsyn, "Dissipative dispersion-managed solitons in mode-locked lasers," Opt. Lett. **34**(21), 3286–3288 (2009).
31. D. Y. Tang, L. M. Zhao, B. Zhao, and A. Q. Liu, "Mechanism of multisoliton formation and soliton energy quantization in passively mode-locked fiber lasers," Phys. Rev. A **72**(4), 043816 (2005).
32. Y. Wang, J. Li, B. Zhai, Y. Hu, K. Mo, R. Lu, and Y. Liu, "Tunable and switchable dual-wavelength mode-locked Tm^{3+}-doped fiber laser based on a fiber taper," Opt. Express **24**(14), 15299–15306 (2016).
33. Z. Yan, H. Wang, K. Zhou, Y. Wang, W. Zhao, and L. Zhang, "Broadband Tunable All-Fiber Polarization Interference Filter Based on 45° Tilted Fiber Gratings," J. Lightwave Technol. **31**(1), 94–98 (2013).
34. D. Y. Tang, W. S. Man, H. Y. Tam, and P. D. Drummond, "Observation of bound states of solitons in a passively mode-locked fiber laser," Phys. Rev. A **64**(3), 033814 (2001).
35. Y. Wang, J. Li, E. Zhang, K. Mo, Y. Wang, F. Liu, X. Zhou, and Y. Liu, "Coexistence of noise-like pulse and high repetition rate harmonic mode-locking in a dual-wavelength mode-locked Tm-doped fiber laser," Opt. Express **25**(15), 17192–17200 (2017).

1. Introduction

Group-velocity dispersion (GVD) in passively mode-locked fiber laser plays a key role for pulse regimes. Generally, conventional soliton (CS) and DS will be respectively formed at large anomalous and normal net cavity GVD regions, where the former is dominated by the balance of nonlinearity and anomalous GVD [1], but the latter mainly depends on the interplay of nonlinear gain and loss [2]. Compared with CS, energy flux of dissipative system across DS produces strong chirp and thus large pulse duration of tens of picosecond level [3]. When mode-locked laser is dispersion managed with segments of positive and anomalous GVD components, the pulse duration of soliton will periodically broaden and compress in the laser cavity and result in increased average pulse duration and higher pulse energy [4, 5]. Especially, in the case of dispersion management with near zero net cavity GVD, SP characterized by high stretching ratio will be formed with narrow pulse duration of femtosecond level [5], where the mechanisms of CS and DS will coexist and compete with

Optics EXPRESS

each other [6]. Dissipative soliton resonance with feature of wave-breaking free can also be formed by properly setting the net cavity dispersion [7]. In these pulse regimes, the GVD is usually treated as wavelength insensitive due to their weak TOD and narrow spectrum range, and as a result the study of strong TOD on mode-locked pulse behavior is rarely reported. In fact, when mode-locked oscillator operates with strong TOD, the GVD becomes greatly wavelength dependent and inevitably give mode-locked pulses some additional features [8–10]. Usually, mode-locked pulses in this case develop asymmetric temporal and spectral profiles owing to the combined effect of GVD and TOD [10–12]. When the GVD is appropriately set, the TOD can even lead to compressing or broadening of pulse duration [11, 13]. Chaotic and quasi-periodic pulse regimes have also been reported with strong TOD in mode-locked lasers [14, 15].

Some fascinating coexistence patterns have also been delivered from mode-locked oscillator with appropriate GVD. L. Wang has demonstrated the coexistence of bright pulses and dark solitons in an Er-doped mode-locked fiber laser with large normal GVD [16]. X. Liu has demonstrated the coexistence of strong and weak pulses in large anomalous GVD region at 1.5 μm band [17]. Although these reports reveal such appealing coexistence patterns through designing suitable net cavity GVD, further exploring of complex coexistence patterns based on strong TOD even higher order dispersion is still unexplored as we best known. Here we numerically and experimentally demonstrate the coexistence of DS and SP by introducing strong TOD with a 10 m dispersion compensation fiber (DCF) in a dual-wavelength mode-locked Tm-doped fiber laser. The performance of the coexistence patterns is investigated in detail.

2. Experiment setup and mechanism

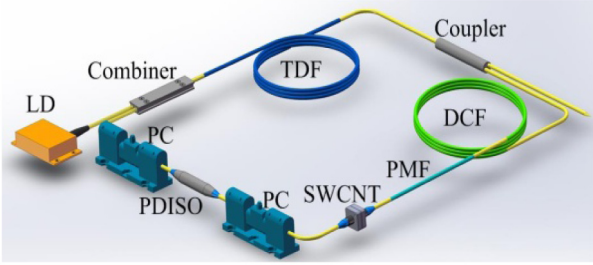

Fig. 1. Setup of dual-wavelength mode-locked fiber laser.

Figure 1 shows the experimental setup. The ring fiber cavity with a total length of ~20.2 m is composed of 1.5 m Tm-doped double-cladding fiber (Coractive, DCF-TM-10/128), 8.5 m SMF 28e fiber, 10 m DCF (OFS, LP980), and 0.2 m polarization maintained fiber (PMF). The Tm-doped fiber served as a gain medium is pumped by a 793 nm diode lasers (BWT) with a max output power of 6 W via a (2 + 1) × 1 pump combiner (ITF, Canada). The DCF is used to compensate the net cavity GVD and induce strong TOD effect. A polarization dependent optical isolator (PDISO) with a polarization extinction ration of 35 dB at 2 μm (Advanced Photonics, USA) is used to induce nonlinear polarization evolution (NPE) effect and ensure the unidirectional propagation. Two polarization controllers (PCs) are used to control the mode-locking performance. The 0.2 m PMF with beat length of 5.3 mm at 1950 nm is adopted to induce comb filter effect which served as a wavelength selector for the multi-wavelength operation [18–20]. The comb filter period is calculated to be 51.2 nm according to the formula of $\Delta\lambda = \lambda L_B/L_{PMF}$, where λ is the center wavelength, L_B and L_{PMF} are the length and beat length of the PMF respectively [21]. Note that the mode-locked fiber laser without the PMF always operates at single-wavelength mode-locking, suggesting that all fibers in the cavity have a weak birefringence coefficient except the PMF. The mode-competition of multi-wavelength operation is suppressed by the wavelength-dependent loss of

Optics EXPRESS

the NPE effect [22]. 20% port of a 2/8 coupler is used as output port. A single-wall carbon nanotube (SWCNT) sandwiched between two optical ferrules is served as a slow saturable absorber (SA) to self-start and stabilize the mode-locking [23]. The measured modulation depth, nonsaturable loss and saturation intensity of the SWCNT SA are 21.2%, 59.6% and 2.23 MW/cm^2, respectively.

Table 1. Measured GVD and TOD of three kinds of fibers at 1950 nm.

Fiber type	GVD (ps^2/km)	TOD (ps^3/km)
Tm-doped fiber	–84	0.3
SMF 28e	–80	0.3
DCF	85	1.67

The output signal is detected by an InGaAs photodetector (EOT ET-5000F, USA) connected to a 500 MHz digital oscilloscope and a radiofrequency (RF) spectrum analyzer, respectively. Interference autocorrelator (APE Pulsecheck USB 150, Germany) and optical spectrum analyzer (Yokogawa AQ6375, Japan) are used to measure the pulse duration and optical spectrum. Since the GVD and TOD of the fiber laser play a key role in our experiment, we measure them with interferometric method [24]. Table 1 lists the measured results. Among them, the DCF with a strong TOD of 1.67 ps^3/km is the main contributor of the net cavity TOD. The net cavity TOD is calculated to be ~0.02 ps^3 at 1950 nm. Stronger TOD effect can be induced by using longer DCF in the cavity. However, when we increase the length of DCF from 10 m to 20 m, the stationary pulse regime becomes unstable and easily switches into noise-like pulse regime because of the long laser cavity and high nonlinearity coefficient of the DCF. With the same reason, even if the laser operates in stationary soliton regime, both the DS and SP will split into a number of sub-pulses due to the strong pulse splitting effect. Therefore, only 10.0 m DCF is used in our experiment.

3. Simulation modeling

Numerical simulation is performed based on coupled extended Ginzburg-Landau equations [25]. The coupled equations are expressed by

$$\begin{cases} \dfrac{\partial U}{\partial z} = i\beta U - \delta\dfrac{\partial U}{\partial t} - \dfrac{i\beta_2}{2}\dfrac{\partial^2 U}{\partial t^2} + \dfrac{\beta_3}{2}\dfrac{\partial^3 U}{\partial t^3} + i\gamma\left(|U|^2 + \dfrac{2}{3}|V|^2\right)U + \dfrac{i\gamma}{3}V^2U^* + \dfrac{g}{2}U + \dfrac{g}{2\Omega_g^2}\dfrac{\partial^2 U}{\partial t^2} \\ \dfrac{\partial V}{\partial z} = -i\beta V + \delta\dfrac{\partial V}{\partial t} - \dfrac{i\beta_2}{2}\dfrac{\partial^2 V}{\partial t^2} + \dfrac{\beta_3}{2}\dfrac{\partial^3 \mathrm{V}}{\partial t^3} + i\gamma\left(|V|^2 + \dfrac{2}{3}|U|^2\right)V + \dfrac{i\gamma}{3}U^2V^* + \dfrac{g}{2}V + \dfrac{g}{2\Omega_g^2}\dfrac{\partial^2 V}{\partial t^2} \end{cases} \quad (1)$$

where, U and V are envelopes of the optical pulses along the two orthogonal polarization axes of the fiber. $2\beta = 2\pi\Delta n/\lambda$ is the wave-number difference between the two modes. $2\delta = 2\beta\lambda/2\pi c$ is the group velocity difference between the two polarization modes. β_2 donates the GVD coefficient. γ refers to the cubic refractive nonlinearity of the medium. $\Omega_g = 2\pi c\Delta\lambda/\lambda^2$ is the bandwidth of the laser gain. The variable T and z are the time and the propagation distance, respectively. g is the net gain, which is nonzero only for the gain fiber. It describes the gain function of Tm doped fiber and is expressed by $g = g_0\exp(-E_P/E_S)$, where g_0 is the small-signal gain, E_P is the pulse energy, and E_S is the gain saturation energy which is pump power dependent. An arbitrary small pulse is served as initial signal to repeatedly propagate in the ring fiber cavity until the optical field becomes self-consistent. When the signal passes through the polarizer, the intensity transmission function is expressed as

$$T = \sin^2(\theta)\sin^2(\varphi) + \cos^2(\theta)\cos^2(\varphi) + 0.5\sin(2\theta)\sin(2\varphi)\cos(\varphi_{PC} + \varphi_{\text{Birefringence}} + \varphi_{NL}) \quad (2)$$

Where θ is the angle between the polarization direction of the light and the fast axis of the birefringent fiber, φ is the angle between the orientation of polarizers and the fast axis of the birefringent fiber. φ_{PC}, $\varphi_{\text{Birefringent}}$ and φ_{NL} are the phase delays induced by polarization controllers, fiber birefringent and nonlinearity effect, respectively. Among them, $\varphi_{\text{Birefringent}}$

Optics EXPRESS

and φ_{NL} are crucial for the mode-competition suppression of multi-wavelength operation because they are wavelength dependent. The filter depth is decided by the term of $\sin(2\theta)\sin(2\varphi)$. Finally, the SWCNT is simulated by the simple two-level saturable absorber model [26]:

$$\alpha(I) = \alpha_{ns} + \frac{\alpha_0}{1 + I / I_{sat}} \tag{3}$$

where $\alpha(I)$ is the intensity-dependent absorption coefficient, and α_0, α_{ns} and I_{sat} are the linear limit of saturable absorption, nonsaturable absorption, and saturation intensity, respectively.

Predictor-corrector split-step Fourier method is adopted to precisely solve the Eq. (1) [27]. Like the experiment setup, the numerical cavity is composed of a polarizer + 8.5 m SMF_fiber + 1.5 m Tm_fiber + 0.5 m SMF_fiber + 2/8 output coupler + 1.5 m SMF_fiber + 10 m DCF + 1 m SMF_fiber + 0.2 m PMF + 1 m SMF_fiber + SA + 1.5 m SMF_fiber. The time window is 896 ps with time step of 54.7 fs. The center wavelength is set to 1950 nm. Beat length of PMF and other fibers are set to 5.3 mm and 1 m respectively. The nonlinearity coefficient of the gain fiber, DCF and SMF28e are respectively set to be 0.8 $W^{-1}m^{-1}$, 0.8 $W^{-1}m^{-1}$, and 4.4 $W^{-1}m^{-1}$. The GVD and TOD of these fibers are the same as Table .1. Gain bandwidth Ω_g and small-signal gain g_0 are respectively set to be 30 THz and 6 m^{-1}. For SWCNT SA model, α_0 = 38.5%, α_{ns} = 58.3% and I_{sat} = 2.23 MW/cm^2 are used. To reflect general physical behaviours of the coexistence patterns, we simplify the numerical model by ignoring some inessential parameters such as insertion loss of all components and higher order dispersion of fiber.

4. Simulation results

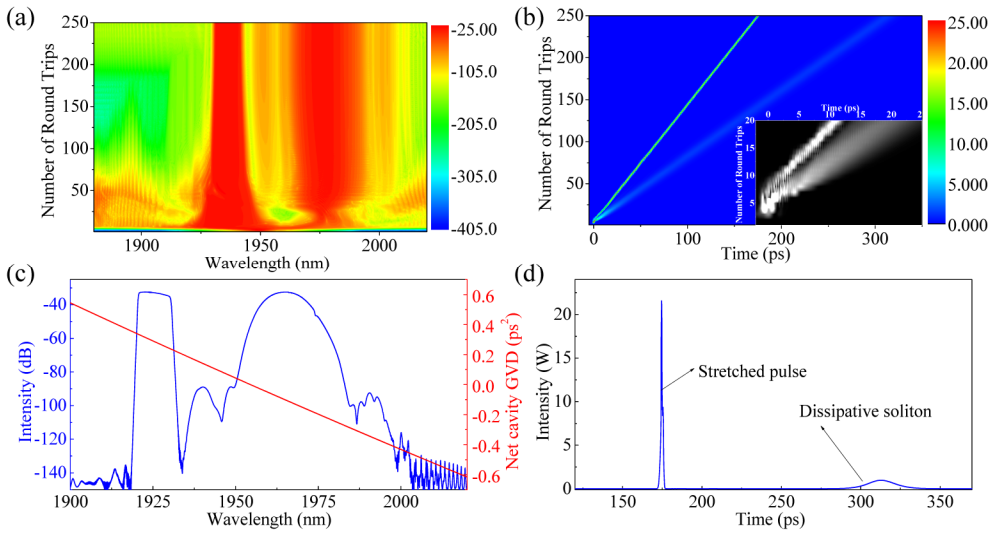

Fig. 2. Simulation of coexistence of DS and SP: (a) and (b) are spectrum and waveform evolution as a function of round-trip number, (c) and (d) are optical spectrum and waveform at round-trip number of 250. Red line in (c) is calculated net cavity GVD as a function of wavelength. Inset of (b) is a zoom-in of the waveform evolution within the round-trip number of 0-20.

In the simulation, increasing of the gain saturation energy E_S corresponds to enhance pump strength [28]. Both θ and φ are set to 0.5π to maximize the filter depth so that the comb filter can effectively induce the multi-wavelength mode-locking. By setting φ_{PC} = 1.7π, stable dual-wavelength mode-locking is obtained when E_S increases to 130 pJ. Note that the center wavelength separation of dual-wavelength mode-locking in our simulation less than the com

Optics EXPRESS

filter period since the laser wavelength at each filter channel tends to close the gain center of the Tm-doped fiber. Figure 2(a) presents the spectrum evolution as a function of round-trip number at the E_S of 150 pJ. Stable spectrum evolution is formed after the round-trip number of ~150. The sub-spectra centered at 1925.7 nm and 1964.5 nm show different intensity distributions. The corresponding evolution of its waveform is presented in Fig. 2(b). The two pulse trains, as shown in inset of Fig. 2(b), start from the same initial weak pulse and quickly split into two pulses with completely different peak intensities and durations. The different evolution slopes of the two pulse trains suggest their different propagation velocities. According to the evolution in Fig. 2(b), the calculated separation between the two pulses increases ~550 fs per round trip. With the assumption of 10.0 MHz repetition rate (decided by cavity length) for one of the two pulses, their repetition rate difference is calculated to be 55 Hz, indicating that the two pulses collide with each other 55 times per second in principle. In the simulation, however, because the 896 ps time window far less than the actual time window of ~100 ns (~1/10MHz), the colliding frequency is up to ~605 kHz in fact. With such high colliding frequency, if the simulation of the coexistence patterns is performed with round number trips of 1000, the both pulses will cross the one side of the time window and come into the time window again from another side, and consequently they will collide with each other. After colliding, interestingly, the both pulses completely maintain their original pulse waveform and phase, indicating that no any modulation or energy exchange occur during the colliding process and they simply obeys the linear superposition principle and independent propagation principle of light wave. Figure 2(c) and 2(d) respectively show the spectrum and waveform at the round number trip of 250. In Fig. 2(c), the sub-spectrum at 1964.5 nm with Gauss profile implies the operation of SP regime, while the other sub-spectrum at 1925.7 nm with steep edges and flat top reflects the feature of DS regime. Weak asymmetry of the spectrum profiles of the DS and SP are caused by strong TOD effect of the laser cavity. Their 3 dB bandwidth are calculated to be 9.6 nm and 9.9 nm, respectively. The weak disturbance formed at the wavelength of 1974.0 nm is sign of Kelly sideband, which caused by resonant enhancement between dispersive wave and soliton is a powerful evidence of SP or CS regime GVD [29]. The Kelly sideband with strong intensity can be obtained when φ_{PC} and E_{sat} are adjusted. Figure 2(c) also shows the calculated net cavity GVD in the wavelength range of 1900 nm to 2020 nm according to the approximate formula of $\beta_3 \approx d\beta_2/d\omega$, where β_2 and β_3 are net cavity GVD and TOD respectively. The calculated GVD decreases from normal to anomalous region toward long wavelength direction. The DS and SP operate at 1925.7/1964.5 nm respectively have corresponding normal/anomalous GVD values of 0.41 ps^2/-0.30ps^2. Due to the different pulse regimes, their waveforms also exhibit contrasting features, as shown in Fig. 2(d): the SP shows narrow pulse duration of 830 fs and high peak power of 20 W, but the DS has large pulse duration of 19.8 ps and low peak power of only 0.98 W.

In order to further validate the features of the DS and SP of the coexistence patterns, we investigate their pulse evolutions along the laser cavity, as shown in Fig. 3(a) and (b). During the evolution, although the pulses change their velocities at different segments, they don't overlap and interact with each other because of their large pulse separation of ~140 ps. As a comparison, the SP shows narrower pulse duration with obvious broadening and compressing behaviour relative the DS. To better clarify, we plot their pulse duration evolutions along the laser cavity in Fig. 3(c) and 3(d). In Fig. 3(c), the high stretching ratio of 3.7 from 2.43 ps at 1.64 m to 660 fs at 0.38 m reflects the typical 'stretching' feature of the SP. Compared with

Optics EXPRESS

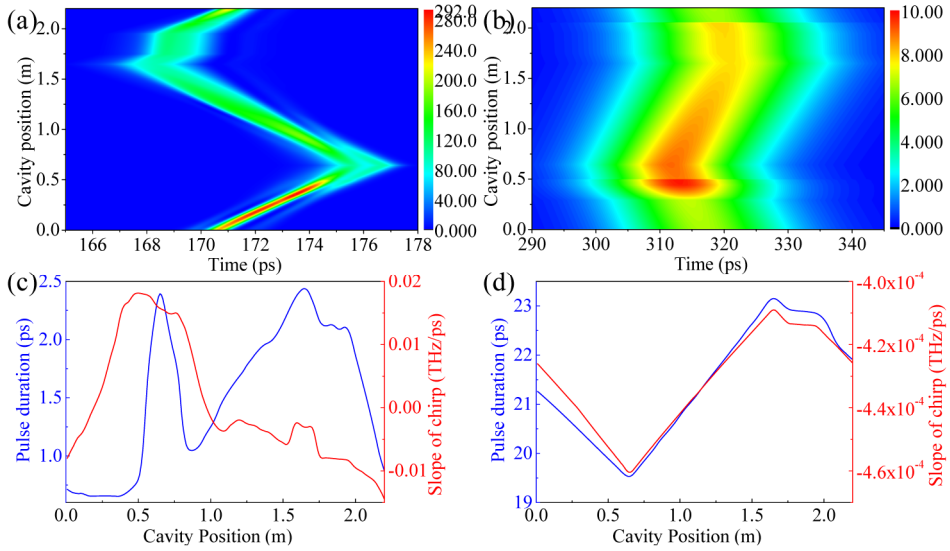

Fig. 3. Evolution of coexistence of DS and SP inside the laser cavity: (a) and (b) are waveform evolution of SP and DS as a function of laser cavity position, respectively, (c) and (d) are corresponding calculated results of pulse duration and slope of chirp at pulse center region.

the SP, the stretching ratio of DS in Fig. 3(d) is only 1.2 calculated by 23.1 ps at 1.65 m to and 19.5 ps at 0.65 m. Besides, the DS and SP respectively stretch and compress once and twice per cavity round trip, and the chirp sign, as indicated in Fig. 3(c) and 3(d) by their chirp slopes at the pulse center region, always maintains negative for DS but varies between both signs for SP. All these keep accordance with the reported features of DS and SP [4, 5, 30].

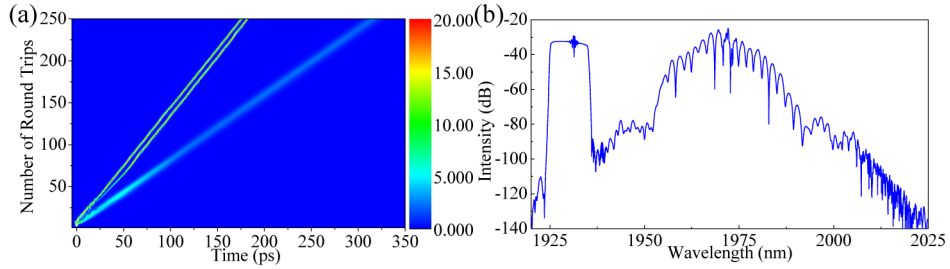

Fig. 4. Simulation of coexistence of DS and bounded SPs: (a) waveform evolution as a function of round-trip number, (b) optical spectrum at round-trip number of 250.

The SP in the coexistence patterns is easily broken into multiple SPs due to its low wave-breaking threshold leaded by its high pulse peak power. Figure 4(a) shows an instance of this case, where the SP is broken into two sub-pulses. The two SPs have nearly identical waveform as a result of soliton energy quantization mechanism in multi-soliton formation [31]. The separation between the two SPs keep constant when the evolution becomes stable, indicating that they belong to bounded SPs. Figure 4(b) shows the corresponding optical spectrum. The spectrum of SP shows obvious modulation which is the typical feature of pulse splitting. Note that the SP will split into more sub-pulses if the E_S further increases, whereas the DS always operate at single pulse regime.

Optics EXPRESS

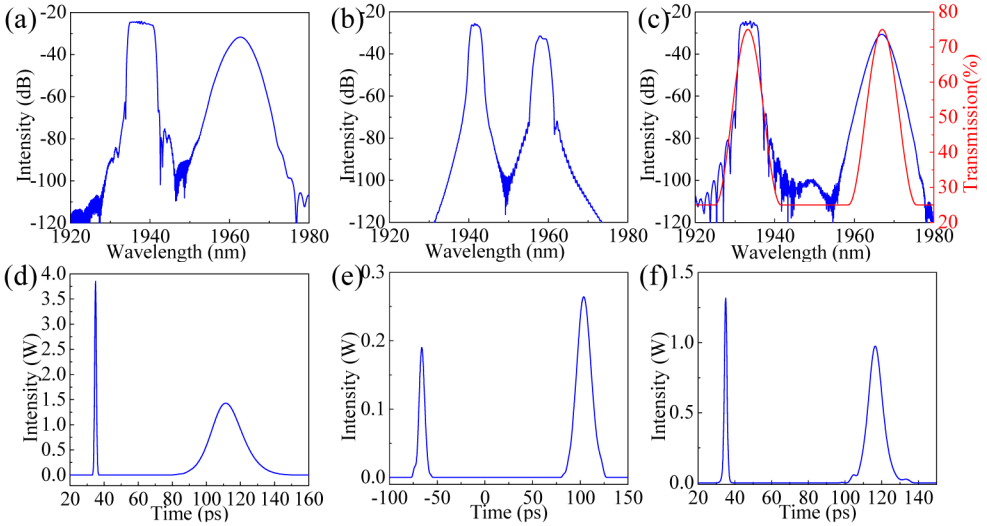

Fig. 5. Simulation of spectra and waveforms of the coexistence of DS and SP with different types of filters: (a) and (b) are spectra based on comb filter with 0.3 m and 0.6 m PMF, respectively, (c) is spectrum with an artificial dual-bandpass filter. (d), (e) and (f) are waveforms corresponding to (a), (b) and (c) respectively. Red curve in (c) is the transmission of the dual-bandpass filter, where the center wavelength separation between the neighboring channels is twice of the comb filter period with 0.6 m PMF.

In the simulation, we find that the comb filter period has important influence on the performance of the coexistence patterns. When we shorten the PMF, the mode-locking tends to operate at single-wavelength regime due to the limited gain bandwidth of 30 THz and limited modulation depth of 50% of the comb filter. Therefore, we only investigated the performance of the coexistence patterns with longer PMF. Figure 5(a) and 5(d) respectively show the pulse spectrum and waveform of the coexistence patterns with 0.3 m PMF. Because the filter period decreases to 34.5 nm in this case, the 3 dB bandwidths of the DS and SP respectively reduce to 6.4 nm and 4.2 nm, and the SP pulse duration dramatically extends to 1.2 ps. In addition, the required value of E_S in this case drops down to 90 pJ because the decreased pulse splitting threshold of the SP with a narrow filter period. When we further increases the length of PMF to 0.6 m, net cavity GVD difference between the neighbouring wavelength channels becomes smaller, and the features of DS and SP become obscure and exhibit some similar feature with each other. Figure 5(b) shows a typical spectrum of this case at E_S of 28 pJ with $\varphi_{PC} = 1.3\pi$, where, instead of SP, a sub-spectrum with basically flat top and steep edges is formed. Because of the narrow comb filter period of 17.2 nm, their pulse durations, as shown in Fig. 5(e), are calculated to be 2.7 ps and 8.9 ps, respectively. Note that the coexistence patterns with typical spectral features of DS and SP can still be obtained by enlarging the center wavelength separation of the dual-wavelength mode-locking without expanding the comb filter period. In order to validate that, we replace the PMF with an artificially set dual-bandpass filter, as shown in Fig. 5(c) with red curve, where its center wavelength separation expands to 34.4 nm but the passband width is the same as the comb filter with 6 m PMF. Blue curve in Fig. 5(c) shows the simulation spectrum of this case, where the dual-wavelength mode-locked pulses at neighboring channels will respectively operate with adequate normal/anomalous net cavity GVD, and typical DS and SP are formed again. Their corresponding waveforms are shown in Fig. 5(f). Compared with Fig. 5(e), the pulse duration of SP is compressed to 1.7 ps.

Optics EXPRESS

5. Experiment results and comparisons

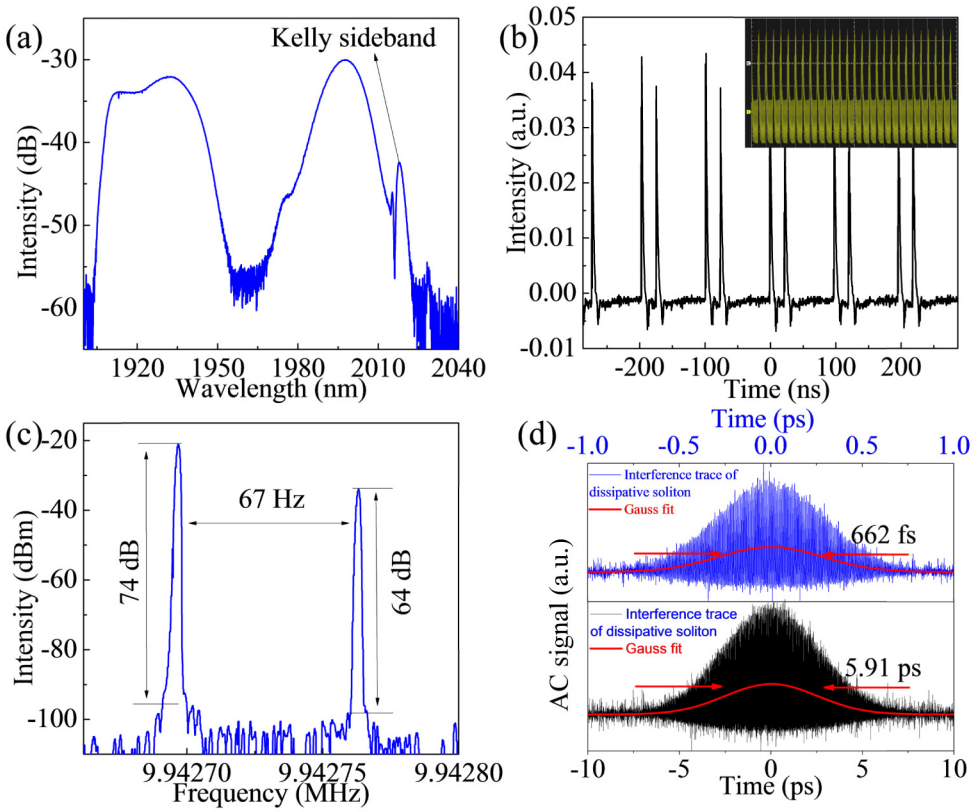

Fig. 6. Experimental results of coexistence of DS and SP with 0.2 m PMF: (a) optical spectrum (b) oscilloscope trace with a scanning range of 600 ns, (c) RF spectrum with a scanning range of 150 Hz, (d) interference autocorrelation traces of the DS (bottom) and SP (top) with scanning range of 20 ps and 2 ps respectively. Inset of (b) is snapshot of the oscilloscope trace of the coexistence patterns.

With ~0.2 m PMF in the fiber cavity, the coexistence of DS and SP is observed by carefully adjusting the PCs and pump power. The output power in this case is 16.3 mW. Note that this coexistence patterns are very sensitive to PCs' position and environmental disturbance because of the difficulty of mode competition suppression in dual-wavelength mode-locking with large comb filter period of 51.6 nm. In addition, with the large comb filter period, mode-competition of the dual-wavelength mode-locking is in fact suppressed by the combined functions of NPE induced wavelength-dependent loss and unflattened gain of Tm-doped fiber, and as a result the center wavelength separation of the dual-wavelength mode-locking is not only decided by the comb filter period of 51.6 nm. Note that the unflatteness of the gain profile can also be validated by our previous work with a fiber taper filter based dual-wavelength mode-locking [32], where the gain unflatteness is a reasonable explain for mode competition suppression because no any additional measure is used. Here, by carefully adjusting the PCs, the coexistence patterns with a large center wavelength separation of 73.8 nm is obtained, which is greatly different from the simulation where unflattened property of gain fiber is ignored. Figure 6(a) shows the optical spectrum in this case, where the dual-wavelength mode-locking centered at 1923.6 nm and 1997.4 nm respectively show the feature of DS and SP regime with 3dB bandwidths of 31.4 nm and 13.85 nm. The SP shows weak Kelly sidebands at 2017 nm, which only appear in the long-wavelength side of the SP due to the strong TOD effect. The DS/SP operates at 1923.6/1997.4 nm has estimated

Optics EXPRESS

normal/anomalous group delay values of 0.12 ps^2/-0.19 ps^2. Compared with simulated spectrum in Fig. 2(c), the DS spectrum in Fig. 6(a) slightly losses its features of flat top and steep edges, which might be caused by the uncontrollable modulation depth of the comb filter in our experiment. In order to estimate the average power of the DS and SP, we respectively calculate their integral scale in Fig. 6(a) with the formula of $\int_{\lambda_1}^{\lambda_2} I(\lambda)d\lambda$, where $I(\lambda)$ is the spectrum intensity distribution of the coexistence patterns, [λ_1 λ_2] is the wavelength range of DS or SP. With the calculated scales of 52% and 48% for the DS and SP, their average powers are respectively estimated to be 8.47 mW and 7.82 mW. Figure 6(b) shows the corresponding oscilloscope trace, where two pulse trains are formed simultaneously. Due to the higher pulse average power of the DS, we deduce that the pulses with high amplitude in the oscilloscope trace correspond to the DS trace. Inset of Fig. 6(b) shows a snapshot of the oscilloscope trace of the coexistence patterns with scan range of 2.8 μs, where once one pulse train is triggered, another pulse train will move randomly on the oscilloscope screen, indicating that the two pulse trains have different propagation velocities [21]. This point can also be validated by their RF spectrum, as shown in Fig. 6(c) with a scanning range of 150 Hz and resolution of 1 Hz, where two fundamental repetition rates with a separation of 67 Hz are formed, which basically matches with the simulation result in Fig. 2(b). Their signal-noise-ratio of better than 60 dB suggests the good stability of the coexistence patterns. In order to measure the pulse duration of the DS and SP, a Lyot-filter is connected before the autocorrelator to respectively extract each of them. To reduce the distortion of the extracted pulse spectrum, the centre wavelength and bandwidth of the filter are controlled by adjusting the temperature and length of the PMF [33]. Figure 6(d) shows the measured traces of the two pulse train with scanning range of 20 ps and 2 ps, respectively. Their pulse durations are respectively measured to be 4.18 ps and 468 fs if Gauss fit is assumed. The time-bandwidth-product of the DS and SP are respectively calculated to be 10.63 and 0.49, indicating that they are all chirped. With the calculated pulse duration and average power, the peak powers of the DS and SP are respectively estimated to be 203 W and 1.68 kW. Note that although their peak powers and pulse durations are very different with the simulation results in Fig. 2 due to the simplified numerical mode, the pulse durations and high peaks power of the DS and SP always show sharp contrast in both experiment and simulation.

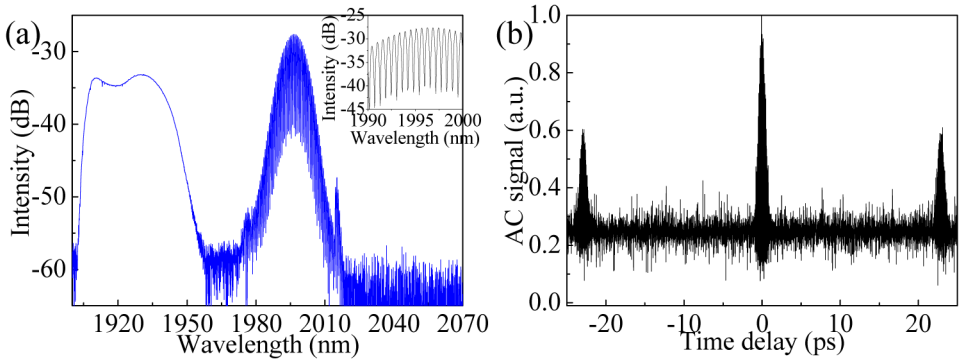

Fig. 7. Experimental results of coexistence of DS and bounded SPs with 0.2 m PMF: (a) (see Visualization 1 and Visualization 2) optical spectrum and (b) interference autocorrelation traces of the bounded SPs with scanning range of 50 ps. Inset of (a) is a zoom-in of the spectral fringe from 1990 nm to 2000 nm.

Like the simulation, the SP in the coexistence patterns can easily operate at multi-pulse state if the PCs or pump strength is changed. Figure 7(a) shows an example of this case, where the SP shows obvious spectral modulation, suggesting that the broken SP pulses are bounded with each other [34]. Inset of Fig. 7(b) shows a zoom-in of the spectral fringe from

Optics EXPRESS

1990 nm to 2000 nm, where the modulation period is calculated to be ~0.59 nm. The DS in this case still operate in single pulse regime. Figure 7(b) shows the corresponding autocorrelation trace of the SP, where the side pulses around the main pulse also indicates the regime of bounded SPs. The separation of 23 ps between the main peak and sub-peak matches well with the spectrum modulation period of ~0.59 nm.

The performance of the coexistence patterns is investigated by gradually increasing the length of PMF. As the length of PMF increases from 0.2 m to 0.6 m, the required pump strength of the coexistence patterns reduces from 1.9 W to 1.2 W, and the pulse duration of SP quickly increases to picosecond level, which matches well with simulation results. Here we present the performance of the coexistence patterns with 0.6 m PMF. Unlike the coexistence

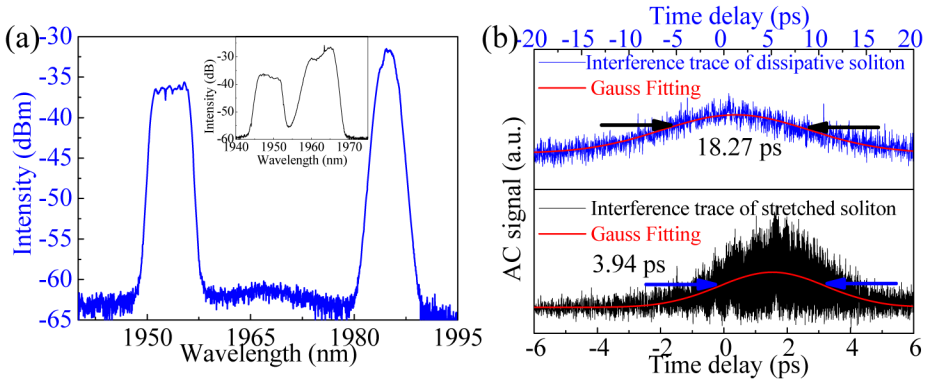

Fig. 8. Experimental results of coexistence of DS and bounded SPs with 0.6 m PMF: (a) optical spectrum with center wavelength separation of 31 nm, (b) interference autocorrelation traces of the DS (top) and SP (bottom) with scanning range of 40 ps and 12 ps respectively. Inset of (a) is dual-wavelength mode-locking with center wavelength separation of ~15 nm.

patterns with 0.2 m PMF, the coexistence patterns in this case become self-started (See Visualization 1). The spectrum evolution switching from single-wavelength operation to dual-wavelength mode-locking during the self-start evolution keeps accordance with our previous works [32 ,35]. Spectrum modulation of the SP indicates the pulse splitting. Stable coexistence patterns without pulse splitting are formed under appropriate pump strength. Visualization 2 shows an example of the stable operation of the coexistence patterns without pulse splitting, where the spectrum stably operates. Figure 8(a) shows a stable-state spectrum of Visualization 2, where the center wavelengths of DS and SP are 1953.6 and 1984.9 nm respectively. Their separation of 31.3 nm is twice of the comb filter period of 17.5 nm, which attributes to the unflattened gain of Tm-doped fiber. With the total average power of 5.4 mW, the average powers of the DS and SP are calculated to be 2.2 mW and 3.2 mW respectively. By adjusting PCs and pump power, dual-wavelength mode-locking is also observed at neighbouring comb filter channel, as shown in inset of Fig. 8(a). However, like simulation, their spectrum profiles show similar feature with each other, indicating that the net cavity GVD difference between neighbouring wavelength channel is too small to form obviously different pulse regimes. Figure 8(b) shows the measured autocorrelation traces. Here autocorrelation traces present weak signal response and loss their fringes due to their weak average powers. With this, the pulse duration of DS and SP are estimated to be 12.9 ps and 2.8 ps with Gauss fit, respectively. Their peak power are calculated to be 17 W and 115 W. Compared with the SP in Fig. 6, the pulse duration and peak power of SP in this case is dramatically changed, indicating that the comb filter period surely has importance limitation on pulse duration of the SP in the coexistence patterns.

Optics EXPRESS

6. Conclusion

We numerically and experimentally demonstrate the coexistence of DS and SP regimes in a dual-wavelength mode-locked Tm-doped fiber laser with strong TOD. Due to the coexistence of different types of pulse shaping mechanism, the pulse durations and peak powers of DS and SP show sharp contrast. In the case of dual-wavelength mode-locking with 0.2 m PMF, coexistence of 4.18 ps DS and 468 fs SP is observed experimentally. Compared with DS, the SP shows low pulse splitting threshold and can easily split into multi-pulses. The comb filter period decided by the length of PMF is crucial for the performance of the coexistence patterns: although large filter period is favorable for the formation of narrower pulse duration of SP, narrow filter period ensures its stability and self-start feature. Single wavelength mode-locked pulse with combined features SP and DS is also presented to suggest the strong TOD effect.

Funding

National Natural Science Foundation of China (Grant No. 61722503, 61435003 and 61421002), Fundamental Research Funds for the Central Universities (Grant No. ZYGX2016J068), and International Scientific Cooperation Project of Sichuan Province (No. 2017HH0046).

192.38.67.116 (ts 2018-07-30 07:28:17)